

Some notes on the program GKINT: Transient-field g -factor kinematics at intermediate energies

Andrew E. Stuchbery

*Department of Nuclear Physics, Australian National
University, Canberra, ACT 0200, Australia**

(Dated: October 28, 2018)

Abstract

This report describes the computer program GKINT, which was developed to plan, analyze and interpret the first High Velocity Transient Field (HVTF) g -factor measurements on radioactive beams produced as fast fragments. The computer program and these notes were written in September 2004. Minor corrections and updates have been added to these notes since then. The experiment, NSCL experiment number 02020, *Excited-state configurations in ^{38}S and ^{40}S through transient-field g -factor measurements on fast fragments*, was performed in October 2004; results have been published in Physical Review Letters 96, 112503 (2006).

arXiv:nucl-ex/0609032v1 21 Sep 2006

*Tel. + 61 2 6125 2097, fax + 61 2 6125 0748, email:andrew.stuchbery@anu.edu.au

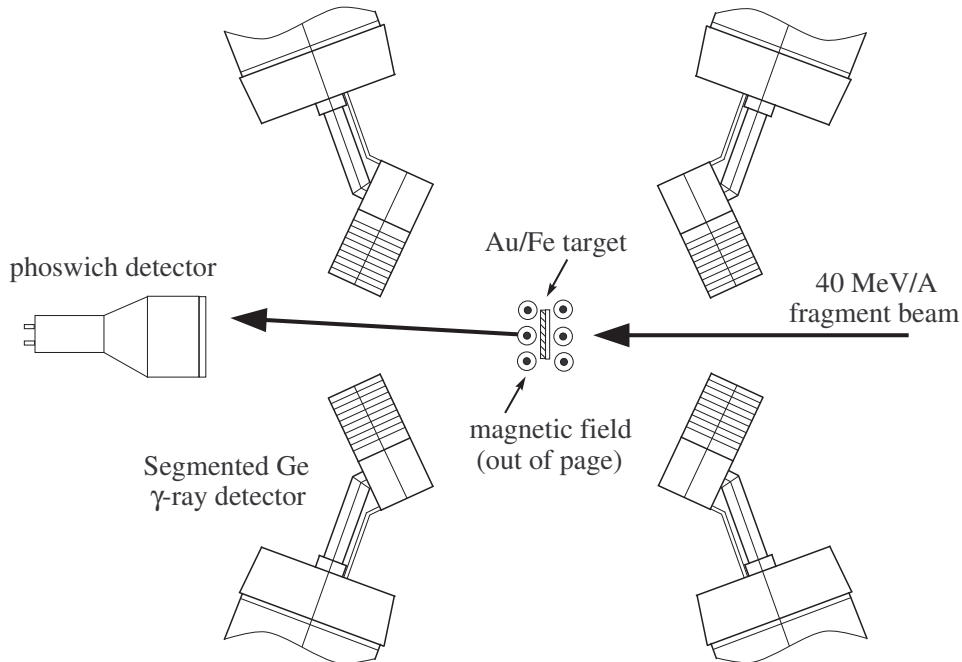


FIG. 1: Schematic view of the experimental arrangement viewed from above. Only the four SeGA detectors perpendicular to the magnetic field axis are shown. There are ten other SeGA detectors which are not shown for clarity.

I. INTRODUCTION

This report contains notes on the code GKINT. Much of the code was based on previous programs for evaluating angular correlations and kinematics in transient-field g factor measurements. These notes therefore tend to put an emphasis on the new features that have been introduced into GKINT. Figure 1 shows the experimental arrangement that the code is written to model.

II. OUTLINE OF THE PROGRAM GKINT

The code GKINT (G factor Kinematics at INTermediate energies) is based on previous codes written at ANU to evaluate the quantities of interest in transient-field g factor measurements. The new features include (i) the use of relativistic kinematics (ii) Coulomb excitation calculations of cross sections and angular correlation parameters appropriate for intermediate energies.

The target can have up to 10 layers of compound composition. One layer has to be specified as the ferromagnetic host. In the present version of the code, the ferromagnetic layer is assumed to be Fe. Apart from the excitation of the 2_1^+ state of Fe, which is hard-wired into the code, calculations can also be performed for any other ferromagnetic host. (If the ferromagnet does not have $Z = 26$ this part of the calculation is skipped. At present the intermediate energy code used is not a coupled-channels code. It cannot evaluate multiple excitation, which might be needed for a valid calculation of the excitation of the rotational Gd isotopes, even in glancing collisions.)

The main tasks performed by the code, in order, are:

1. Read in all input data.
2. Trace energy loss of beam through all target layers.
3. Calculate projectile Coulex and angular correlation parameters as a function of energy-loss through the target at the average scattering angle.
4. Do detailed calculations of projectile Coulex cross sections, count rates, Doppler-shift parameters, angular correlation parameters, transit times, ion energies/velocities through each layer, transient-field precessions, etc., taking into account both the finite solid angle of the particle counter and the energy loss of the beam in the target.
5. Evaluate angular correlations and perturbed angular correlations, including RIV effects, at the angles of the Segmented germanium array (SeGA).
6. Evaluate cross sections and angular correlations for excitation of the Fe target layer.

III. ENERGY LOSS

A. Energy loss algorithm

Energy loss of the beam in the target layers is evaluated using the stopping power formulation of Ziegler et al. (1985). These stopping powers appear to be quite accurate for S beams in Au and Fe targets. A provision is made to scale to stopping powers for each layer by an input parameter.

Because the stopping powers are a function of energy, the energy loss calculations have to be done by dividing the target layer into narrow strips of width Δx . To work efficiently with the thick foils that are used here, the energy loss algorithms were improved by using the Runge-Kutta method.

To avoid confusing notation, we put $dE/dx = S(E)$ to denote the energy dependence of the stopping power. If the energy of the ion as it enters the strip n is E_n , then the energy at the next strip E_{n+1} is

$$E_{n+1} = E_n - \Delta E. \quad (1)$$

We have to evaluate ΔE . The Runge-Kutta equations give

$$\Delta E = (\Delta E_1 + 2\Delta E_2 + 2\Delta E_3 + \Delta E_4)/6 \quad (2)$$

where

$$\Delta E_1 = S(E_n)\Delta x \quad (3)$$

$$\Delta E_2 = S(E_n - \Delta E_1/2)\Delta x \quad (4)$$

$$\Delta E_3 = S(E_n - \Delta E_2/2)\Delta x \quad (5)$$

$$\Delta E_4 = S(E_n - \Delta E_3)\Delta x \quad (6)$$

The Runge-Kutta method gives an exact solution (but for rounding errors) when $S(E)$ can be represented by a polynomial of degree not greater than four. Convergence is tested by repeating the calculation with double the number of steps. The energy loss converges within a few keV for targets several hundred mg/cm² thick when a few hundred steps are used. There can be a reduction in the accuracy if the ion almost stops, but such cases must be avoided in an experiment anyway.

B. Energy loss calculations in GKINT

The first part of the calculation is to evaluate the energy loss of the beam through the target layers. The beam energy at the front of each target layer is determined and the transit time through the layer is evaluated. The energy with which the ion leaves the target is also printed.

For the subsequent integrations, each target layer is then subdivided into a number of strips of equal depth, and the energy of the beam at each strip is evaluated and stored. A

survey of the Coulomb excitation cross sections and angular correlation parameters (a_2 and a_4) as a function of depth is made, assuming that the beam scatters at the average detection angle, $\bar{\theta} = (\theta_{\max} + \theta_{\min})/2$.

In the case of intermediate-energy fragments scattering at small angles, the difference between the incident and scattered beam energies is very small. However it is evaluated precisely, and the subsequent energy loss of the scattered beam ion along its trajectory toward the particle counter is evaluated as a function of depth through the target, as required.

IV. TRANSIENT-FIELD PRECESSIONS

Transient-field precessions are evaluated for ions that traverse the ferromagnetic layer of the target using the routine ROTN. The primary purpose of this routine is to evaluate

$$\phi(\tau) = \Delta\theta/g = -\frac{\mu_N}{\hbar} \int_{T_i}^{T_e} B_{\text{tr}}(t) e^{-t/\tau} dt, \quad (7)$$

where g and τ are the g factor and lifetime of the excited state. B_{tr} is the transient-field strength, which varies with time as the ion slows within the ferromagnet.

The integral over time is rewritten as an integral over energy using the non-relativistic relations

$$dt = dx/v = dx/\sqrt{2E/M} = dE\sqrt{M/2E}/(dE/dx) \quad (8)$$

where E is the energy and M is the mass of the ion. The use of the non relativistic formula for energy is not expected to be too unrealistic because the TF strength is small until the ion velocity falls to around $0.15c$.

In the routine ROTN the integral over the energy range is performed using Simpson's rule. Along with the precession angle, ROTN evaluates a number of other quantities that are often considered useful in relation to the Transient Field.

The effective time for which the ion experienced the TF during its flight through the ferromagnetic foil layer must be evaluated first. From this, one may derive the average ion velocity and the average TF strength.

If t_i and t_e are the times at which the probe ion entered into and exited from the ferromagnetic foil, and τ is the mean life of the probe state, the effective interaction time is

$$t_{\text{eff}} = \tau[\exp(-t_i/\tau) - \exp(-t_e/\tau)]. \quad (9)$$

When $\tau \gg t_i, t_e$,

$$t_{\text{eff}} = t_i - t_e = t_{fe}, \quad (10)$$

where t_{fe} is the time the probe ion takes to traverse the ferromagnetic layer. The average velocity of the ion whilst in transit through the ferromagnet is

$$\langle v/v_0 \rangle = [\int_{t_i}^{t_e} (v/v_0) \exp(-t/\tau) dt] / t_{\text{eff}}, \quad (11)$$

where $v_0 = c/137$ is the Bohr velocity. Again, when the mean life is much longer than the transit time,

$$\langle v/v_0 \rangle = L/[v_0 t_{fe}], \quad (12)$$

where L is the thickness of the ferromagnetic foil. If ϕ is expressed in milliradians and the interaction time in ps, the average TF strength in kTesla is

$$\langle B_{TF} \rangle = 0.0209\phi/t_{\text{eff}}. \quad (13)$$

V. COULEX CALCULATIONS AND PARTICLE KINEMATICS

A. Modifications to COULINT

Coulex cross sections are evaluated using routines from COULINT, written by C.A. Bertulani, see Phys. Rev. C 68, 044609 (2003). A few modifications were needed for the present application.

Firstly, the COULINT routines were modified to return the CM differential cross section for a specified energy and scattering angle. Both the Rutherford and Coulomb excitation cross sections are returned. The code was also modified to return the statistical tensor for the angular correlation in the projectile frame, at the specified energy and particle scattering angle. Since there is some difference in the terminology, and in the definitions of the statistical tensors, the code works with a_k coefficients, which are the coefficients that occur in the familiar Legendre polynomial expansion of the angular correlation:

$$W(\theta_\gamma) = 1 + a_2 P_2(\cos \theta_\gamma) + a_4 P_4(\cos \theta_\gamma) \quad (14)$$

The centre-of-mass to Lab transformations were evaluated with relativistic formulae:

$$\tan \theta_{\text{Lab}} = \frac{1}{\gamma_2} \cdot \frac{\sin \theta_{\text{CM}}}{(\cos \theta_{\text{CM}} + M_p \gamma_1 / M_t \gamma_2)} \quad (15)$$

and

$$\cos \theta_{\text{CM}} = \frac{1}{(1 + \gamma_2^2 \tan^2 \theta_{\text{Lab}})} \left[-\frac{M_p}{M_t} \gamma_1 \gamma_2 \tan^2 \theta_{\text{Lab}} \pm \left(1 - \frac{M_p^2 - M_t^2}{M_t^2} \tan^2 \theta_{\text{Lab}} \right)^{1/2} \right] \quad (16)$$

where the positive sign is the only one relevant in the present work. The notation used here drops the prime that in many references is attached to the factors γ_i . To define these gamma factors it is convenient to introduce $\rho = M_p/M_t$. As usual we have

$$\gamma = (1 - v^2/c^2)^{-1/2} = 1 + T/m_0c^2 \quad (17)$$

where T is the beam energy in MeV per nucleon and $m_0c^2 = 931.494$ MeV. In terms of ρ and γ we have

$$\gamma_1 = \frac{\gamma + \rho}{(1 + 2\rho\gamma + \rho^2)^{1/2}} \quad (18)$$

and

$$\gamma_2 = \frac{1 + \gamma\rho}{(1 + 2\rho\gamma + \rho^2)^{1/2}} \quad (19)$$

The lab cross sections were evaluated as

$$\frac{d\sigma_{\text{Lab}}}{d\Omega_{\text{Lab}}} = \frac{d\sigma_{\text{CM}}}{d\Omega_{\text{CM}}} \cdot \frac{d\Omega_{\text{CM}}}{d\Omega_{\text{Lab}}} \quad (20)$$

The solid angle ratio, evaluated non-relativistically in terms of the particle scattering angles, is

$$\frac{(d\sigma/d\Omega)_{\text{CM}}}{(d\sigma/d\Omega)_{\text{Lab}}} = \frac{d\Omega_{\text{Lab}}}{d\Omega_{\text{CM}}} = \left(\frac{\sin \theta_{\text{Lab}}}{\sin \theta_{\text{CM}}} \right)^2 |\cos(\theta_{\text{CM}} - \theta_{\text{Lab}})| \quad (21)$$

The relativistic formula is

$$\frac{d\Omega_{\text{Lab}}}{d\Omega_{\text{CM}}} = \frac{\gamma_2 [1 + (M_p \gamma_1 / M_t \gamma_2) \cos \theta_{\text{CM}}]}{[\sin^2 \theta_{\text{CM}} + \gamma_2^2 (\cos \theta_{\text{CM}} + M_p \gamma_1 / M_t \gamma_2)^2]^{3/2}} \quad (22)$$

The code uses the proper relativistic evaluation, although the relativistic formulation differs from the non-relativistic one by a negligible factor in many cases.

B. GKINT description: cross sections

Figures 2 and 3 show the variations in the projectile Coulomb excitation and Rutherford cross sections as a function of scattering angle for ^{38}S at 20 and 40 MeV/ A , respectively, incident on ^{197}Au . The figures also show the excitation probability, $P_{i \rightarrow f}$, which is

$$P_{i \rightarrow f} = \frac{(d\sigma/d\Omega)_{i \rightarrow f}}{(d\sigma/d\Omega)_{\text{Rutherford}}} \quad (23)$$

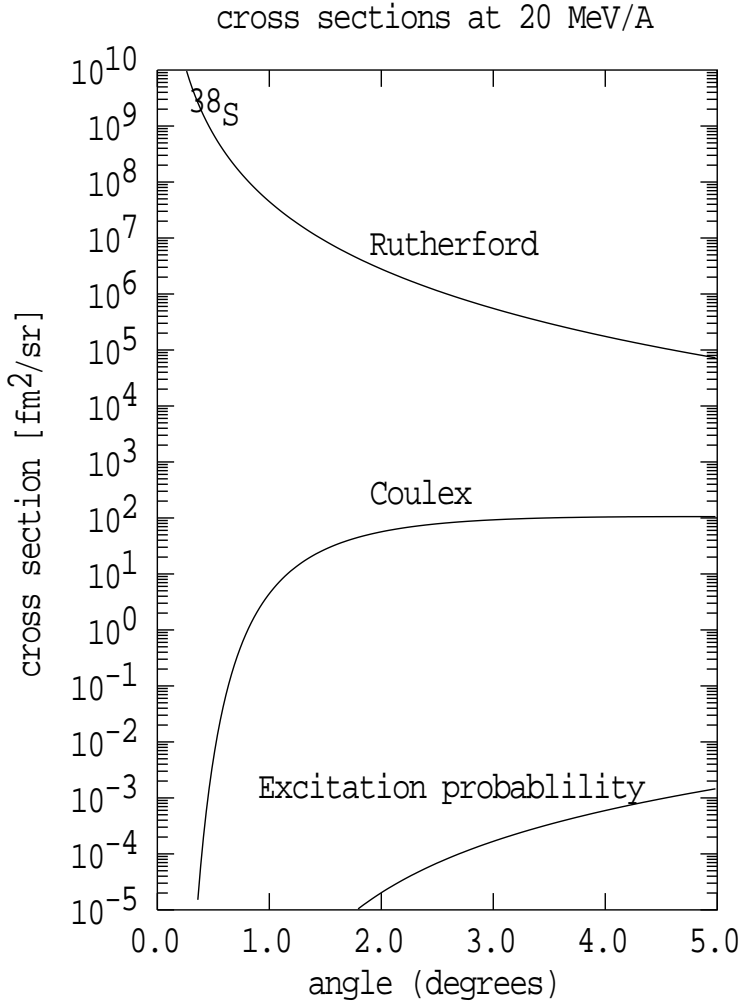


FIG. 2: Cross sections as a function of scattering angle for 20 MeV/A ^{38}S on ^{197}Au .

Note that the Rutherford cross section goes to infinity as the scattering angle approaches zero. The Coulex cross section remains well behaved, however, because $P_{i \rightarrow f}$ approaches zero faster than the Rutherford cross section diverges.

GKINT performs integrals over the solid angle of the particle detector and over the depth of the target:

$$\langle \sigma \cdot t_{\text{tgt}} \rangle = 2\pi \int_0^{t_{\text{tgt}}} \int_{\theta_p^{\text{min}}}^{\theta_p^{\text{max}}} \frac{d\sigma}{d\Omega}(\theta_p, E[z]) \sin \theta_p d\theta_p dz, \quad (24)$$

where the scattering angles and the cross section are in the lab frame, and z denotes the depth through the target. With the cross sections in fm^2 and target thickness in mg/cm^2 , the count rate R in Hz is

$$R = N_{\text{beam}} \langle \sigma \cdot t_{\text{tgt}} \rangle \frac{N_A}{A} \quad (25)$$

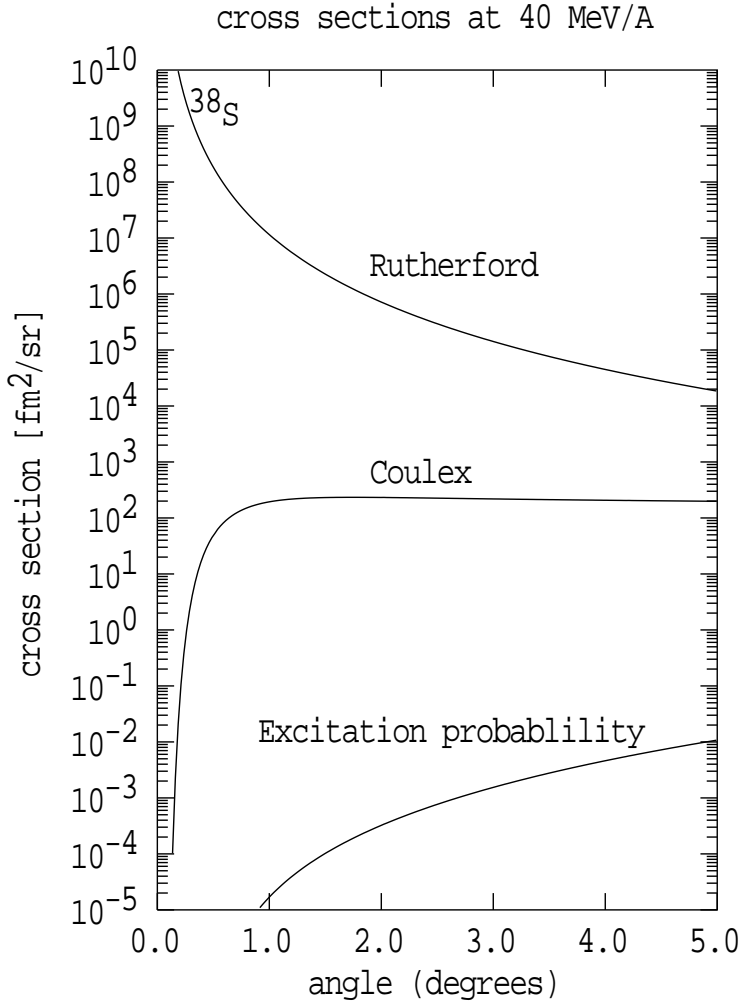


FIG. 3: Cross sections as a function of scattering angle for 40 MeV/A ^{38}S on ^{197}Au .

$$= (6.023 \times 10^{-6}) N_{\text{beam}} \frac{\langle \sigma \cdot t_{\text{tgt}} \rangle}{A}, \quad (26)$$

where N_{beam} is the number of beam ions/sec, N_A is Avagadro's number, and A is the atomic mass number. The count rates for Coulomb excitation and Rutherford scattering as registered by the particle counter are printed for $N_{\text{beam}} = 1000$. If the Rutherford cross section is in the region where it diverges and thus implies $R > N_{\text{beam}}$, which is clearly unphysical, the code puts $R = N_{\text{beam}}$ and prints a warning.

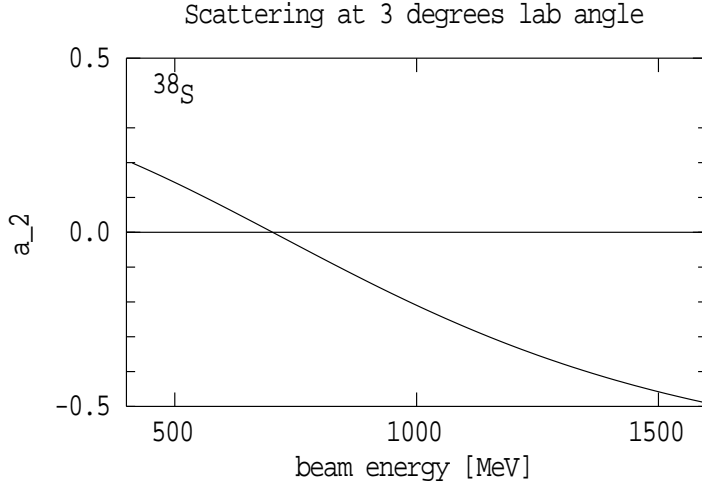


FIG. 4: a_2 angular correlation coefficient as a function of beam energy at a lab scattering angle of 3° for ^{38}S on ^{197}Au .

C. GKINT description: angular correlation coefficients

The spin alignment in intermediate energy Coulomb excitation depends on both the beam energy and the scattering angle. As can be seen in Fig. 4, the alignment decreases as the beam energy decreases, eventually changing sign. Similar behavior is evident when a_2 is plotted as a function of the scattering angle, Fig. 5. Again the alignment decreases with scattering angle, eventually changing sign.

For each layer of the target, the average a_k coefficients are evaluated as

$$\langle a_k \rangle = \frac{2\pi}{\langle \sigma \cdot t_{\text{tgt}} \rangle} \int_0^{t_{\text{tgt}}} \int_{\theta_p^{\text{min}}}^{\theta_p^{\text{max}}} a_k(\theta_p, E[z]) \frac{d\sigma}{d\Omega}(\theta_p, E[z]) \sin \theta_p d\theta_p dz. \quad (27)$$

The integrals are performed numerically using Simpson's rule.

Similar integrals are performed to evaluate the average energy of excitation, the average transient-field precessions, etc. In each case the quantity to be averaged replaces a_k in an expression of the same form as Eq. (27).

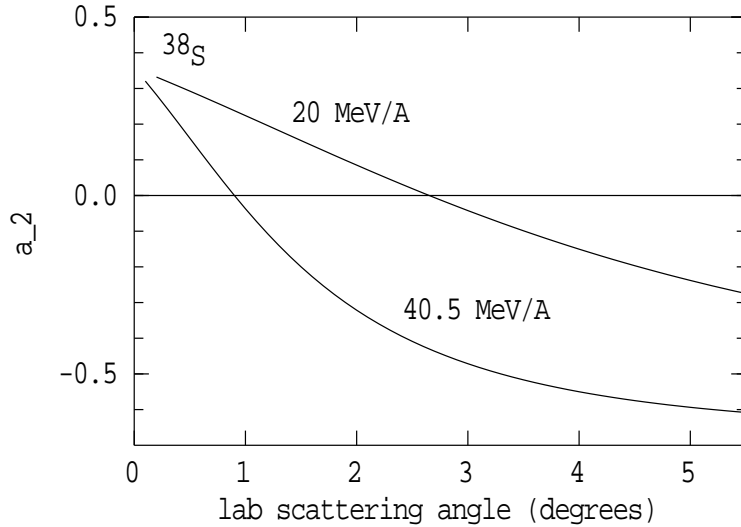


FIG. 5: a_2 angular correlation coefficient as a function of lab scattering angle for ^{38}S on ^{197}Au .

VI. ANGULAR CORRELATION FORMALISM

The theoretical expression for the unperturbed angular correlation after Coulomb excitation in general can be written as

$$W(\theta_\gamma, \phi_\gamma) = \sum_{k,q} \sqrt{(2k+1)} \rho_{kq}(\theta_p, \phi_p) F_k G_k Q_k D_{q0}^{k*}(\phi_\gamma, \theta_\gamma, 0), \quad (28)$$

where $\rho_{kq}(\theta_p, \phi_p)$ is the statistical tensor which defines the spin alignment of the initial state, and depends on the particle scattering angles (θ_p, ϕ_p) , F_k represents the usual F -coefficients for the γ -ray transition, G_k is the vacuum deorientation attenuation factor, Q_k is the attenuation factor for the finite size of the γ -ray detector and $D_{q0}^k(\phi_\gamma, \theta_\gamma, 0)$ is the rotation matrix, which depends on the γ -ray detection angles $(\theta_\gamma, \phi_\gamma)$. The Coulex calculation uses a right-handed co-ordinate frame in which the beam is along the positive z -axis. In the applications of interest $k = 0, 2, 4$.

Since we are interested in the case where the particle detector has azimuthal symmetry, the statistical tensors ρ_{kq} depend only on θ_p and are non-zero only when $q = 0$:

$$\rho_{kq}(\theta_p, \phi_p) = \delta_{q,0} \rho_{k0}(\theta_p) \quad (29)$$

The program GKINT integrates the Coulex cross sections over the opening angle of the

particle detector and evaluates the a_k coefficients defined as

$$a_k = \sqrt{(2k+1)\rho_{k0}}F_k \quad (30)$$

In the experiments a magnetic field will be applied in the vertical direction, along the x -axis or $\phi = 0$ direction. We define FIELD UP as being when the external field points UP along the positive x -axis. The transient-field precession is given by

$$\Delta\theta = g\phi = -g\frac{\mu_N}{\hbar} \int_{T_i}^{T_e} B_{\text{tr}}(t)e^{-t/\tau} dt, \quad (31)$$

where g is the nuclear g factor, τ is the meanlife of the level, and T_i and T_e are the times at which the ion enters into and exits from the ferromagnetic foil. (This expression corresponds to the precession information in the whole gamma-ray lineshape, including decays which occur while the nucleus is still in motion through the ferromagnet. The code also evaluates the precession for those nuclei that decay in vacuum after leaving the ferromagnetic layer of the target.) The important point to note here is that the precession angle, $\Delta\theta$, is *negative* for a positive field (i.e. field UP) and a positive g factor.

Now consider that the nucleus undergoes a transient-field precession of $\pm\Delta\theta$ as the external field is alternatively flipped up and down. We set aside the question of whether the positive precession corresponds to field-up or field-down, since we don't know the sign of the g factor a priori. The statistical tensor is then modified by the precession about the field axis, according to

$$\rho_{kq}(\pm\Delta\theta) = \sum_Q \rho_{kQ}\delta_{Q,0}D_{qQ}^k(\pi/2, \pm\Delta\theta, -\pi/2) \quad (32)$$

$$= \rho_{k0}D_{q0}^k(\pi/2, \pm\Delta\theta, 0) \quad (33)$$

$$= \rho_{k0}D_{q0}^k(\pm\pi/2, |\Delta\theta|, 0) \quad (34)$$

$$= \rho_{k0}\sqrt{\frac{4\pi}{(2k+1)}}Y_q^k(|\Delta\theta|, \pm\pi/2) \quad (35)$$

In GKINT it is convenient to work with spherical harmonics rather than the rotation matrices. To get the final form of the perturbed angular correlation we need to use

$$D_{q0}^k(\alpha, \beta, \gamma) = \sqrt{\frac{4\pi}{(2k+1)}}Y_q^k(\beta, \alpha) \quad (36)$$

and

$$Y_q^{k*}(\beta, \alpha) = (-1)^q Y_{-q}^k(\beta, \alpha) \quad (37)$$

Note that, depending on the implementation in the computer routine, putting a negative β value in the D matrix, and/or the spherical harmonic, may not be properly interpreted. We will therefore avoid doing it in the code.

We then get the final expression for the perturbed angular correlation which GKINT uses:

$$W(\theta_\gamma, \phi_\gamma, \pm\Delta\theta) = 4\pi \sum_{k,q} \frac{a_k Q_k G_k}{(2k+1)} (-1)^q Y_q^k(|\Delta\theta|, \pm\pi/2) Y_{-q}^k(\theta_\gamma, \phi_\gamma) \quad (38)$$

The evaluation of the vacuum deorientation parameters, G_k , is discussed below. At present the gamma detector solid angle factors Q_k are all set to unity. We will need to formulate a procedure to evaluate these in future (perhaps using GEANT). However the detectors are sufficiently far from the target that $Q_k = 1$ is a reasonable first approximation.

VII. LORENTZ CORRECTION FOR γ RAYS

Because we have azimuthal symmetry, the Lorentz correction in this case is quite straightforward. The basic formulae, which have been written in many publications, are reviewed in the first subsection. In the second subsection the method of treating the perturbed angular correlation is discussed. I'm not aware of any place in the literature where this situation is discussed in any detail.

A. Formulae for angular correlations

The angle between the beam axis and the direction of emission of the photon is affected if the nucleus is in motion rather than at rest. The relativistic velocity addition formulae can be used to show that the angles of emission in the laboratory, $(\theta_{\text{lab}}, \phi_{\text{lab}})$, are related to those in the rest frame of the nucleus, $(\theta_{\text{nuc}}, \phi_{\text{nuc}})$, by the expressions

$$\cos \theta_{\text{lab}} = \frac{\cos \theta_{\text{nuc}} + \beta}{1 + \beta \cos \theta_{\text{nuc}}}, \quad (39)$$

and

$$\phi_{\text{lab}} = \phi_{\text{nuc}}, \quad (40)$$

where $\beta = v/c$ is the velocity of the nucleus along $\theta_{\text{lab}} = \theta_{\text{nuc}} = 0$. It follows that an element of solid angle in the rest frame is related to an element of solid angle in the laboratory frame

by

$$d\Omega_{\text{lab}} = \frac{1 - \beta^2}{(1 + \beta \cos \theta_{\text{nuc}})^2} d\Omega_{\text{nuc}}. \quad (41)$$

To obtain the correlation in the laboratory frame, $W_{\text{lab}}(\theta_{\text{lab}})$, from that in the rest frame of the nucleus, $W_{\text{nuc}}(\theta_{\text{nuc}})$, requires both transformation of the laboratory angle to the equivalent angle in the rest frame of the nucleus using Eq. (39), and multiplication by the appropriate solid-angle ratio so that the γ -ray flux emitted into 4π of solid angle is conserved, i.e.

$$\int_{4\pi} W_{\text{lab}}(\theta_{\text{lab}}) d\Omega_{\text{lab}} = \int_{4\pi} W_{\text{nuc}}(\theta_{\text{nuc}}) d\Omega_{\text{nuc}}. \quad (42)$$

This condition is satisfied if

$$W_{\text{lab}}(\theta_{\text{lab}}) = W_{\text{nuc}}(\theta_{\text{nuc}}) \frac{d\Omega_{\text{nuc}}}{d\Omega_{\text{lab}}}. \quad (43)$$

B. Formulae for perturbed angular correlations

The precession of the nucleus takes place in the frame of the nucleus (obviously!). However we measure the perturbed angular correlation in the Lab frame.

The standard technique for measuring small transient-field precessions in a way that minimizes possible systematic errors is to form a double ratio of γ -ray intensities for each complementary pair of γ -ray detectors placed at angles $\pm\theta_\gamma$ with respect to the beam direction:

$$\rho = \sqrt{\frac{N(+\theta_\gamma \uparrow) N(-\theta_\gamma \downarrow)}{N(+\theta_\gamma \downarrow) N(-\theta_\gamma \uparrow)}} \quad , \quad (44)$$

where $N(\pm\theta_\gamma \uparrow, \downarrow)$ denote the numbers of counts in the photopeak of the transition of interest as registered in the detectors at $\pm\theta_\gamma$ for the alternative field directions (\uparrow and \downarrow).

The effect of the transient field is to rotate the angular correlation by a relatively small angle around the direction of the applied magnetic field. Thus

$$W(\theta_\gamma \uparrow) = W(\theta_\gamma - \Delta\theta) \simeq W(\theta_\gamma) - \Delta\theta \left. \frac{dW}{d\theta} \right|_{\theta_\gamma}. \quad (45)$$

In the case where there are no (or negligible) Lorentz effects, the precession angle $\Delta\theta$ is determined from

$$\Delta\theta = \frac{\varepsilon}{S} \quad , \quad (46)$$

where

$$\varepsilon = \frac{1 - \rho}{1 + \rho} \quad , \quad (47)$$

and S , the logarithmic derivative of the angular correlation at the angle θ_γ , is

$$S = \left. \frac{1}{W} \frac{dW}{d\theta} \right|_{\theta_\gamma} \quad . \quad (48)$$

To see how these expressions must be modified to account for Lorentz effects, it is convenient to note that ε is formally equivalent to

$$\varepsilon = \frac{W(+\theta_\gamma\downarrow) - W(+\theta_\gamma\uparrow)}{W(+\theta_\gamma\downarrow) + W(+\theta_\gamma\uparrow)} \quad . \quad (49)$$

The perturbed angular correlation in the lab frame is given by

$$W_{\text{lab}}(\theta_{\text{lab}} \uparrow) = W_{\text{nuc}}(\theta_{\text{nuc}} \uparrow) \frac{d\Omega_{\text{nuc}}}{d\Omega_{\text{lab}}} = W_{\text{nuc}}(\theta_{\text{nuc}} - \Delta\theta) \frac{d\Omega_{\text{nuc}}}{d\Omega_{\text{lab}}} \quad . \quad (50)$$

Hence

$$\varepsilon_{\text{lab}} = \frac{W(\theta_{\text{nuc}}\downarrow) - W(\theta_{\text{nuc}}\uparrow)}{W(\theta_{\text{nuc}}\downarrow) + W(\theta_{\text{nuc}}\uparrow)} = \varepsilon_{\text{nuc}} \quad . \quad (51)$$

In the case of the Lorentz boost, the expression for $\Delta\theta$ is

$$\Delta\theta = \frac{\varepsilon_{\text{lab}}}{S_{\text{nuc}}} \quad . \quad (52)$$

Thus the only change in the analysis procedure is that S must be evaluated at the appropriate angle in the rest frame of the nucleus, which corresponds to the laboratory detection angle.

Finally, it is worth noting that if $W(\theta)$ has the form of Eq. (14), then

$$S(\theta) = -(a_2 P_{21}(\cos \theta) + a_4 P_{41}(\cos \theta))/W(\theta) \quad (53)$$

where P_{21} and P_{41} are associated Legendre polynomials.

VIII. RECOIL IN VACUUM ATTENUATION FACTORS

The G_k coefficients are evaluated as follows, based on experimental data and experience at ANU.

For the experiments of interest, with ions emerging into vacuum with velocities near the K -shell electron velocity, the vacuum deorientation is dominated by the fields at the nucleus from the ground-state of the H-like electron configuration, i.e. $1s$ fields. At the

lower velocities of interest $2s$ fields also contribute. In this description, we will begin by assuming that the $1s$ fields are dominant and then introduce the $2s$ contribution at the end. The code uses both.

Neglecting the relativistic correction (which is small for $Z = 16$), the field at the nucleus from the $1s$ electron of an H-like ion is

$$B_{1s} = 16.7Z^3 \text{ Tesla.} \quad (54)$$

This free-ion field causes the nuclear spin I to precess with a Larmor frequency of

$$\omega = g \frac{\mu_N}{\hbar} (2I + 1) B_{1s} \quad (55)$$

The vacuum deorientation coefficients for a pure $1s$ configuration are

$$G_k^{1s} = 1 - b_k \frac{(\omega\tau)^2}{1 + (\omega\tau)^2}, \quad (56)$$

where τ is the nuclear lifetime, and

$$b_k = k(k + 1)/(2I + 1)^2 \quad (57)$$

Thus for $I = 2$ we have $b_2 = 0.24$ and $b_4 = 0.80$. In the worst case for $I = 2$, $G_2^{1s}(\text{hardcore}) = 0.76$, and although $G_4^{1s}(\text{hardcore}) = 0.20$, the $k = 4$ term (a_4) in the angular correlation is already small. In fact, for virtually any reasonable level lifetime (approaching a picosecond or more) and a g -factor value that differs even a little from zero, the hyperfine field is so big that $G_k^{1s} \approx G_k^{1s}(\text{hardcore})$.

We have measured the charge-state fractions for Si and S ions with energies between about 90 MeV and 240 MeV emerging from Fe and Gd. (AES, Anna Wilson and Paul Davidson, Nuclear Instruments and Methods B 243, 265 (2006).) The results for S after Fe are shown in Fig. 6. Near $v = Zv_0$ the 15^+ charge state is dominant. The other prolific charge states in their atomic ground states produce either smaller fields (13^+) or no field at all (14^+ and 16^+). Under these conditions it is reasonable to evaluate the average vacuum deorientation coefficients for the experimental conditions in terms of the fraction of ions that carry a single electron, Q_H . Thus

$$G_k = (1 - Q_H) + Q_H G_k^{1s} \quad (58)$$

After some simple algebra we get

$$G_k = 1 - Q_H b_k \frac{(\omega\tau)^2}{1 + (\omega\tau)^2}. \quad (59)$$

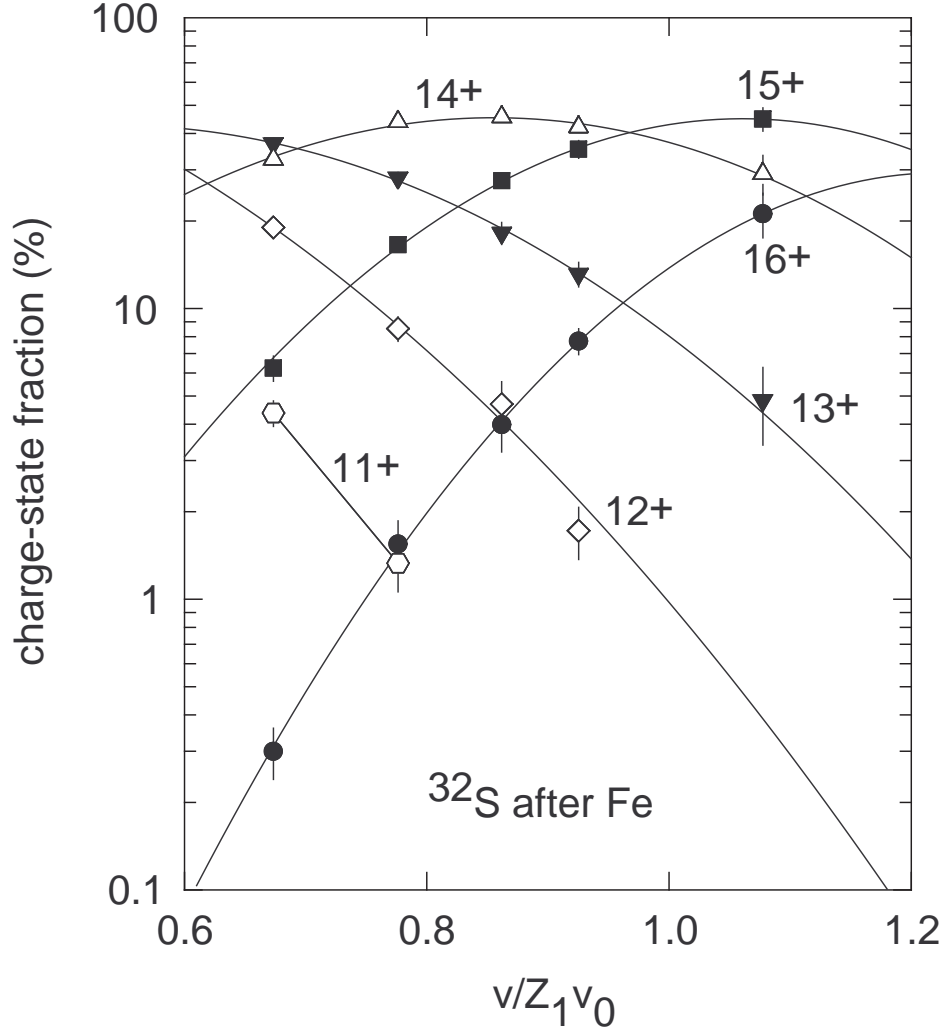


FIG. 6: Charge-state fractions for S ions emerging from Fe as a function of the ion velocity. The highest-velocity point was obtained with beams boosted by the ANU Linac. The curves are based on fits to Eq. (62).

Thus provided that $Q_H < 0.5$, $G_2 > 0.88$ and $G_4 > 0.6$.

For S ions with velocities near $0.7Zv_0$ (100 MeV), the Li-like fields should be included:

$$G_k = 1 - Q_H b_k \frac{(\omega\tau)^2}{1 + (\omega\tau)^2} - Q_{Li} b_k \frac{(\omega\tau/8)^2}{1 + (\omega\tau/8)^2} \quad (60)$$

where Q_{Li} is the lithium-like fraction, and it is assumed that

$$B_{ns} = 16.7Z^3/n^3 \quad \text{Tesla.} \quad (61)$$

TABLE I: Results of fits to Eq. (62) for ions with 3 or fewer electrons.

Beam	Target	q	v/Zv_0 range		Parameters		
			min	max	a_0	a_1	a_2
Si	Fe	14	0.83	1.26	-18.6231	26.2176	-9.6632
		13	0.83	1.26	-9.6665	15.3430	-6.5868
		12	0.83	1.26	-3.1681	7.0924	-4.8990
		11	0.83	1.26	-4.1570	9.5851	-8.0001
S	Fe:	16	0.67	1.08	-23.6376	36.5961	-14.9403
		15	0.67	1.08	-14.9891	26.7520	-12.6089
		14	0.67	1.08	-7.6139	15.9538	-9.3268
		13	0.67	1.08	-3.1411	8.4963	-7.8757
S	Gd	16	0.75	1.08	-17.8000	23.8431	-8.6552
		15	0.64	1.08	-12.7697	20.9555	-9.2347
		14	0.64	1.08	-6.0770	11.9903	-6.6953
		13	0.64	1.08	-2.2632	5.3773	-5.1736
Si	Gd	14	0.80	1.25	-17.9075	23.8099	-8.4427
		13	0.80	1.25	-8.0397	11.4628	-4.4435
		12	0.80	1.25	-5.6947	11.2019	-6.3201
		11	0.80	1.12	0.5950	0.1204	-3.0000

The experimental data for the charge fractions in Fig. 6 were fitted to the form

$$F(q, v/Z_1v_0) = \exp(a_0 + a_1v/Z_1v_0 + a_2(v/Z_1v_0)^2), \quad (62)$$

where the parameters a_0 , a_1 and a_2 are determined for each charge state. The fit parameters for the most prolific charge states are listed in Table I.

The code at present uses the fit to the charge-state results for S after Fe to interpolate the values of Q_H and Q_{Li} and thus obtain as realistic an evaluation of G_k as possible. (It

will give a warning if the ion velocity is outside the region where there are experimental data. The extrapolations must break down because the charge-state distributions are not truly a gaussian function of ion velocity.)

The code uses the expression in Eq. (60) to evaluate the RIV effect. In the cases considered to date, $\omega\tau$ is so large that

$$\frac{(\omega\tau)^2}{1 + (\omega\tau)^2} \approx \frac{(\omega\tau/8)^2}{1 + (\omega\tau/8)^2} \approx 1, \quad (63)$$

and hence, to an excellent approximation,

$$G_k = 1 - (Q_H + Q_{Li})b_k. \quad (64)$$

Cautionary note: We know the form of $G(t)$ for the vacuum deorientation effect, however we measure

$$\langle G_k \rangle = (1/\tau) \int_{t_{exit}}^{\infty} G_k(t) \exp(-t/\tau) dt, \quad (65)$$

where t_{exit} is the time at which the ions emerge into vacuum. The code at present assumes $t_{exit} = 0$ in the evaluation of the $\langle G_k \rangle$, as is the case for Eq. (56). This gives an accurate result if $t_{exit} \ll \tau$. Thus the present calculations for ^{40}S ($\tau \sim 20$ ps) should be fine, while those for ^{38}S ($\tau \sim 5$ ps) might tend to over estimate the vacuum deorientation effect slightly. A more rigorous evaluation of the $\langle G_k \rangle$ value applicable in the experiments is available from the Monte Carlo Doppler Broadened Line Shape (DBLS) code, GKINT_MCDBLS.

IX. SOME PEDAGOGICAL PLOTS OF THE PERTURBED CORRELATIONS

A. TF precessions in the nuclear (projectile) frame

While the effect of the precession is most pronounced for detectors in the horizontal plane, the other planes are also expected to show useful precession effects. The following figures 7 - 9 illustrate how the projectile (or nuclear frame) precession varies with the phi angle of the γ -ray detector.

B. RIV perturbation in the lab frame

Fig. 10 shows the angular correlation in the lab frame with and without the RIV contribution. In this case the particle scattering angle is between 2.5° and 5.5° . The ^{38}S beam

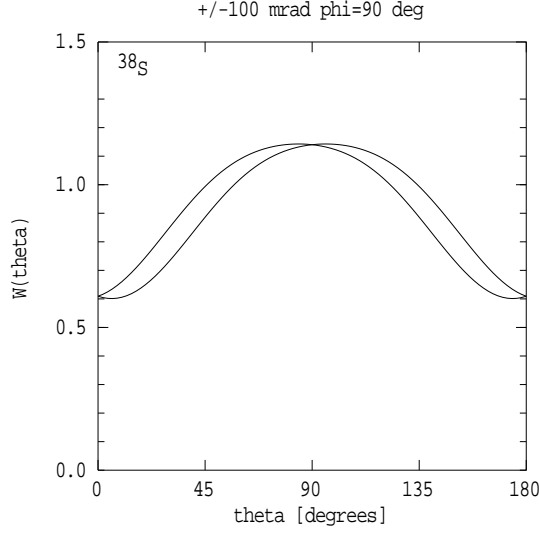


FIG. 7: Perturbed angular correlations in the CM frame as observed in the horizontal, or $\phi = 90^\circ$, plane.

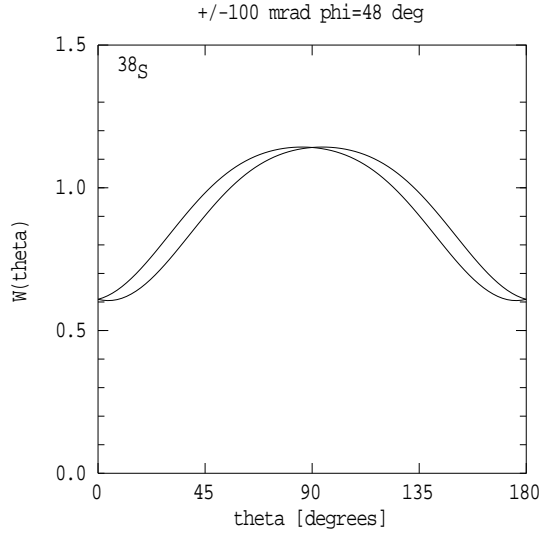


FIG. 8: Perturbed angular correlations in the CM frame as observed in the $\phi = \pm 48^\circ$ or $\phi = \pm 228^\circ$ planes.

energy is 1540 MeV. The unattenuated angular correlation coefficients are $a_2 = -0.4233$ and $a_4 = -0.0990$. For a H-like fraction of $Q_H = 0.1269$ and a Li-like fraction of $Q_{Li} = 0.3108$, $G_2 = 0.8978$ and $G_4 = 0.6595$. The Lorentz effects are evaluated using $\beta = 0.089$.

Note that the RIV effect on the angular correlation is modest and that it is very difficult to measure the RIV attenuation because γ -ray detectors cannot be placed at either 0° or 180°

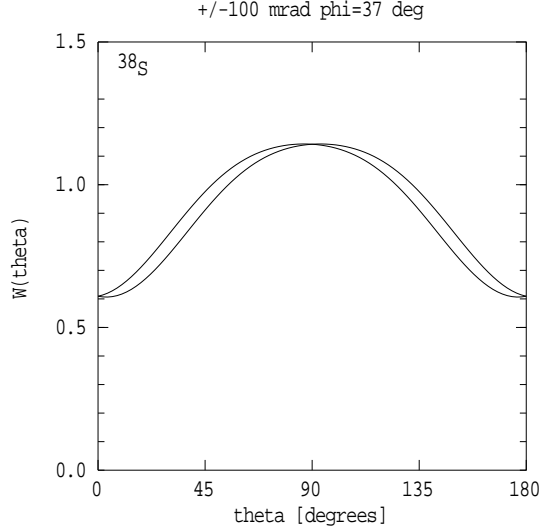


FIG. 9: Perturbed angular correlations in the CM frame as observed in the $\phi = \pm 37^\circ$ or $\phi = \pm 217^\circ$ planes.

to the beam in intermediate-energy Coulomb excitation measurements. The measurements of the charge-state fractions are therefore very important.

X. FIGURE OF MERIT: OPTIMIZING EXPERIMENTAL CONDITIONS

GKINT provides the quantities designated S^2W , S^2N and $S^2\phi^2N$ evaluated at the SeGA detector angles as figures of merit. This section explains the rationale of these choices as figures of merit.

We begin by obtaining an estimate of the experimental error on the measured precession for a given number of accumulated counts in a single pair of detectors. Since the precession angles are relatively small, we can assume that

$$N(+\theta_\gamma, \uparrow) \approx N(-\theta_\gamma, \downarrow) \approx N(+\theta_\gamma, \downarrow) \approx N(-\theta_\gamma, \uparrow) \approx N. \quad (66)$$

Thus N is the total number of counts recorded in *one* detector for *one* field direction. With the further approximation that

$$\sigma_N \approx \sqrt{N}, \quad (67)$$

it follows that

$$\sigma_{\Delta\theta} \approx \frac{1}{2S\sqrt{N}}.$$

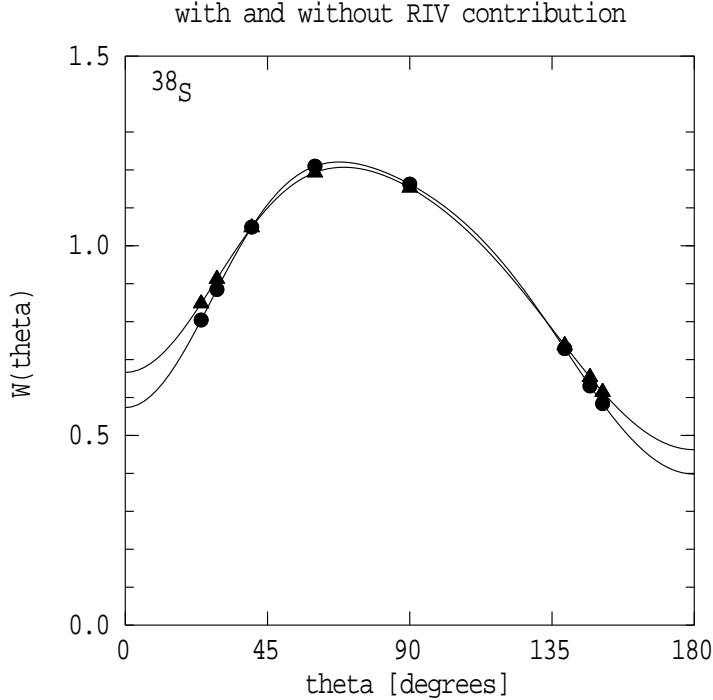


FIG. 10: Angular correlation in the lab frame with and without the RIV contribution.

It is usually more convenient to work with a figure of merit that scales with the number of counts, and hence is inversely proportional to the required beam time. Thus we can calculate quantities proportional to S^2N as the figure of merit and note that we must maximize it for optimum sensitivity.

GKINT calculates both S^2W and $S^2W\sigma$, denoting the latter as S^2N . Generally $S^2N = S^2W\sigma$ will be the quantity of interest. (S^2W is retained in the output to give an indication of the angular correlation contribution, separate from the cross section.) These figures of merit are independent of the magnitude of $\Delta\theta$. Clearly, in a real experiment the goal is to minimize $\sigma_{\Delta\theta}/\Delta\theta$. As another figure of merit GKINT also evaluates

$$S^2\phi^2W\sigma e^{(-T_{\text{exit}}/\tau)}, \quad (68)$$

which is proportional to $(\sigma_{\Delta\theta}/\Delta\theta)^2$ for the fraction of excited nuclei that experience the full transient-field precession and decay in vacuum beyond the target. Here T_{exit} is the average time at which beam ions exit from the target.

The calculations are given with and without the effect of the RIV attenuation. Since the RIV effect can not be avoided, the unattenuated angular correlations are given mainly as a point of reference.

TABLE II: Additional details of the angular correlation in Fig 10 for the case without vacuum deorientation.

posn	θ	ϕ	$d\Omega_{\text{nuc}}/d\Omega_{\text{lab}}$	$W(\theta)_{\text{lab}}$	$S(\theta)$	S^2W
1	24.0	180.0	1.1763	0.8013	0.0000	0.000
2	40.0	131.0	1.1433	1.0459	0.5937	0.369
3	90.0	112.0	0.9920	1.1630	-0.0381	0.002
4	147.0	143.0	0.8584	0.6329	-0.6467	0.265
5	139.0	228.0	0.8705	0.7315	0.6896	0.348
6	60.0	241.0	1.0870	1.2077	-0.2589	0.081
7	151.0	90.0	0.8533	0.5861	-1.1148	0.728
8	151.0	270.0	0.8533	0.5861	1.1148	0.728
9	29.0	91.0	1.1675	0.8816	1.0543	0.980
14	29.0	271.0	1.1675	0.8816	-1.0543	0.980
17	24.0	1.3	1.1763	0.8013	0.0254	0.001
18	60.0	61.0	1.0870	1.2077	0.2589	0.081
19	139.0	46.0	0.8705	0.7315	-0.6675	0.326
20	147.0	323.0	0.8584	0.6329	0.6467	0.265
21	90.0	292.0	0.9920	1.1630	0.0381	0.002
22	40.0	310.0	1.1433	1.0459	-0.6027	0.380

XI. EFFECT OF A MASK ON THE PARTICLE DETECTOR

Table IV summarizes some calculations made to assess the use of different masks on the particle detector. The main benefit of the mask is to reduce the Rutherford rate. The small reduction in Coulex count rate is compensated for by an increase in the anisotropy of the angular correlation.

TABLE III: Additional details of the RIV attenuated angular correlation in Fig 10.

posn	θ	ϕ	$d\Omega_{\text{nuc}}/d\Omega_{\text{lab}}$	$W(\theta)_{\text{lab}}$	$S(\theta)$	S^2W
1	24.0	180.0	1.1763	0.8450	0.0000	0.000
2	40.0	131.0	1.1433	1.0454	0.5165	0.279
3	90.0	112.0	0.9920	1.1536	-0.0468	0.003
4	147.0	143.0	0.8584	0.6562	-0.5152	0.174
5	139.0	228.0	0.8705	0.7404	0.5773	0.247
6	60.0	241.0	1.0870	1.1911	-0.2669	0.085
7	151.0	90.0	0.8533	0.6169	-0.8662	0.463
8	151.0	270.0	0.8533	0.6169	0.8662	0.463
9	29.0	91.0	1.1675	0.9096	0.8472	0.653
14	29.0	271.0	1.1675	0.9096	-0.8472	0.653
17	24.0	1.3	1.1763	0.8450	0.0196	0.000
18	60.0	61.0	1.0870	1.1911	0.2669	0.085
19	139.0	46.0	0.8705	0.7404	-0.5588	0.231
20	147.0	323.0	0.8584	0.6562	0.5152	0.174
21	90.0	292.0	0.9920	1.1536	0.0468	0.003
22	40.0	310.0	1.1433	1.0454	-0.5242	0.287

TABLE IV: Effect of a mask on the particle detector. The calculations are for a standard ^{38}S configuration with $E_{\text{beam}} = 1540$ MeV. The target is 355 mg/cm^2 Au followed by 100 mg/cm^2 . The stopping powers are scaled by a factor of 1.02.

θ_p^{min}	Count rate/1000 beam ions (Hz)		$S^2W\sigma$
	Coulex	Rutherford	
$\theta_p^{\text{max}} = 5^\circ$			
0	0.0596	1000	762
1	0.0598	290	778
2	0.0523	63	856
2.5	0.0466	36	869
3	0.0395	21	836
$\theta_p^{\text{max}} = 5.5^\circ$			
0	0.0720	1000	1119
1	0.0713	292	1138
2	0.0647	66	1236
2.5	0.0589	38	1260
3	0.0518	24	1237